6 El Niño – Southern Oscillation (ENSO)

6.1 Introduction

At irregular intervals of two to seven years, the cold tongue of water along the equator in the eastern Pacific region warms up by as much as 3 K, accompanied by vast changes in atmospheric circulation and the distribution of rainfall over the tropical Pacific and Indian Oceans. These events were well known to pre-Columbian residents of Pacific coastal South America, and Peruvian fishermen referred to such episodes as El Niño events as they tend to occur around Christmas ('El Niño', literally "the boy', referring to the Christ child), bringing large changes to local fish and seabird populations. In contemporary parlance, the opposite phase of the system, perhaps better characterized as the absence of El Niño, is referred to as 'La Niña'.

In the mid-1920s, Gilbert Walker (after whom the Walker Circulation was named) noticed a strong anti-correlation between seasonally varying sea surface pressures at Darwin, Australia, and Tahiti, in the central tropical South Pacific, and coined the term "Southern Oscillation" to describe this see-saw of pressures. Somewhat later it was recognized that the Southern Oscillation and the dramatic warming of the eastern equatorial Pacific are part of the same phenomenon, which is now referred to as ENSO. We use the terms El Niño and La Niña to describe different phases of ENSO.

ENSO is an enormously broad and intellectually extraordinarily rich subject that deserves a textbook of its own; here we provide only a rudimentary overview. The reader is referred to Webster (2020) for a comprehensive review of the scientific understanding of ENSO. Wang et al. (2017) also provide a nice review of the subject.

Examples of the distributions of sea surface temperature anomalies in two different types of El Niño episode are shown in Figure 6.1. These patterns represent the two leading EOF's of ENSO variability (Takahashi et al., 2011) and most El Niño events can be well described as a weighted sum of these two patterns. The eastern Pacific pattern peaks just off the coast of Peru, while the second pattern peaks in the central equatorial Pacific.

The strong sea surface temperature anomalies are associated with equally pronounced circulation anomalies. Figure 6.2 is a schematic diagram showing distributions of surface pressures and winds, superimposed on sea surface temperature anomalies, for the two ENSO phases. El Niño events are associated with strong westerly wind anomalies (and the actual wind can become westerly over large portions of the central and western equatorial Pacific), reduced pressure in the east and increased pressure in the west. As one might expect, the westerly low-level wind anomalies are associated with anomalous ascent in the eastern equatorial Pacific, and descent in the west, and this is reflected in the pattern on anomalous precipitation (Figure 6.3). The precipitation anomalies can be quite large and persist for many months, leading to sever drought in Indonesia, Australia, southeast Asia, and as far away as India, and flooding in equatorial South America.

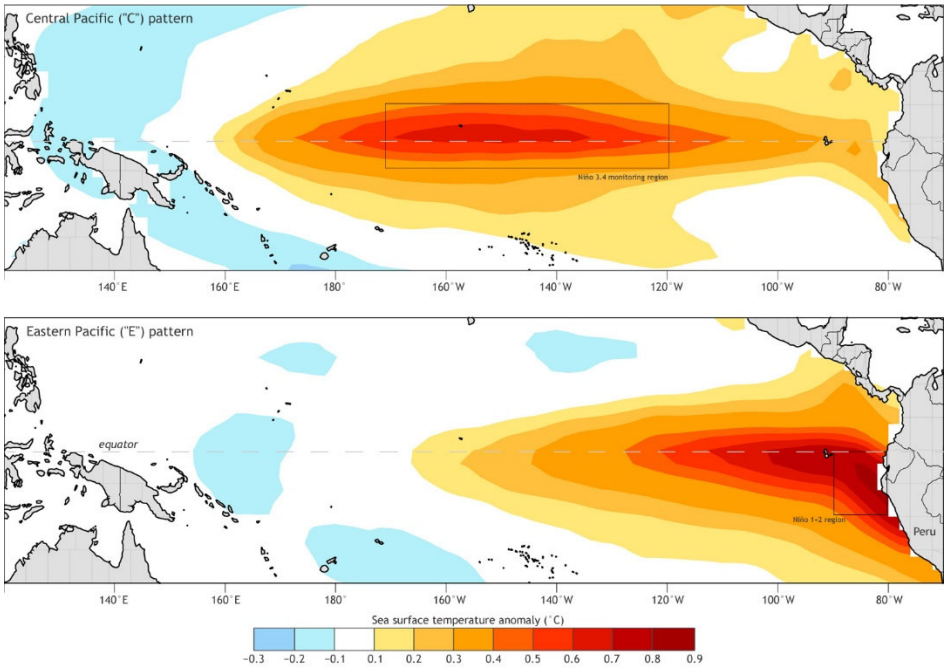

Figure 6.1: Composite sea surface temperature anomalies (K) for two different classifications of El Niño. Top: Central Pacific pattern; Bottom: Eastern Pacific pattern. These represent the two leading empirical orthogonal functions of the ENSO variability, and most El Niño events can be described as a weighted sum of these. The thin black boxes represent conventional ENSO monitoring regions.

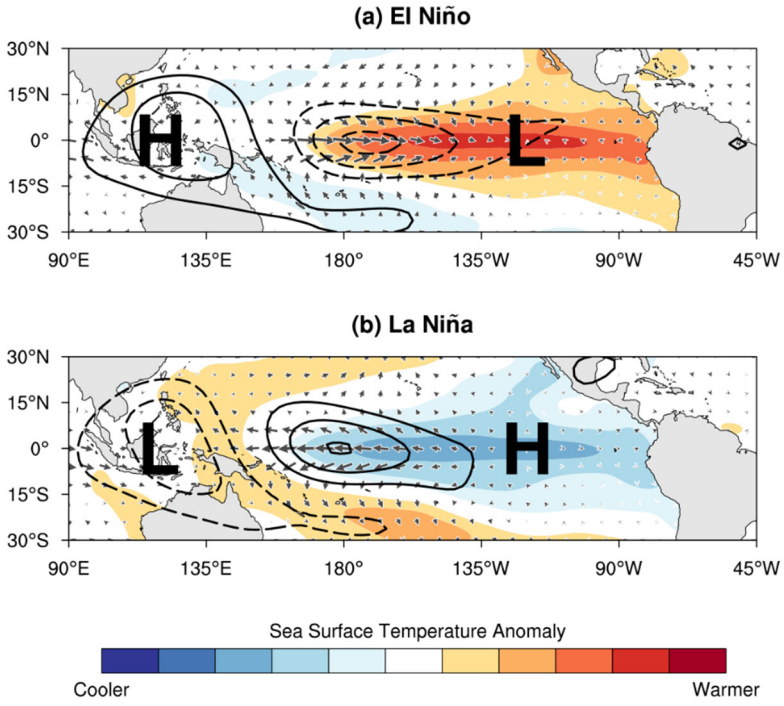

Figure 6.2: Schematic diagram showing the distributions of anomalous surface winds and pressures and associated sea surface temperature anomalies for the two phases of ENSO. The schematic is based on the composite anomalies for November-December drawn from 11 warm events and 11 cold events during 1980-2016.

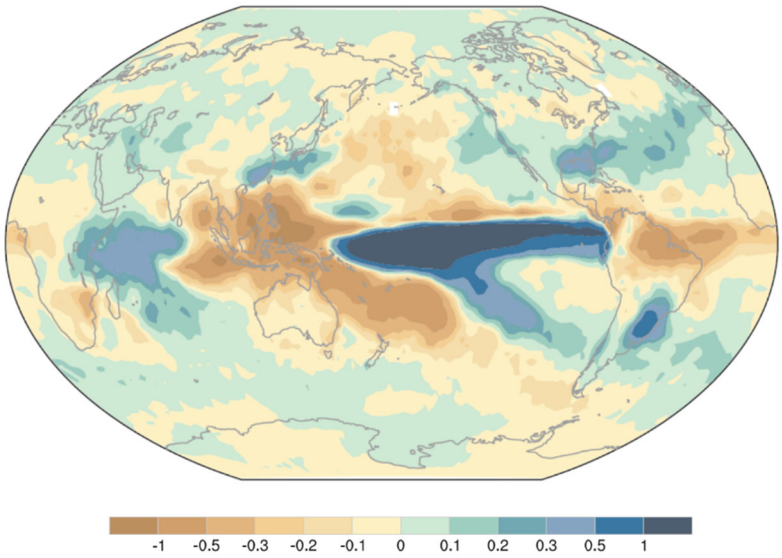

Figure 6.3: Monthly precipitation anomalies regressed onto the first principle component of ENSO time series of sea surface temperature. The precipitation is based on the satellite-based Global Precipitation Climatology Project for the period 1979–2011. Units are mm day-1 per standard deviation of the principle component time series of sea surface temperature.

ENSO is a strongly coupled phenomena, accompanied by strong perturbations in the upper equatorial Pacific Ocean. During El Niño events, the thermocline sinks in the east and rises in the west in association with positive sea surface temperature anomalies in the east and negative in the west (Figure 6.4). This represents a strong relaxation of the normal upward slope of the thermocline toward the east and massive eastward movement of the warm pool waters of the western equatorial Pacific.

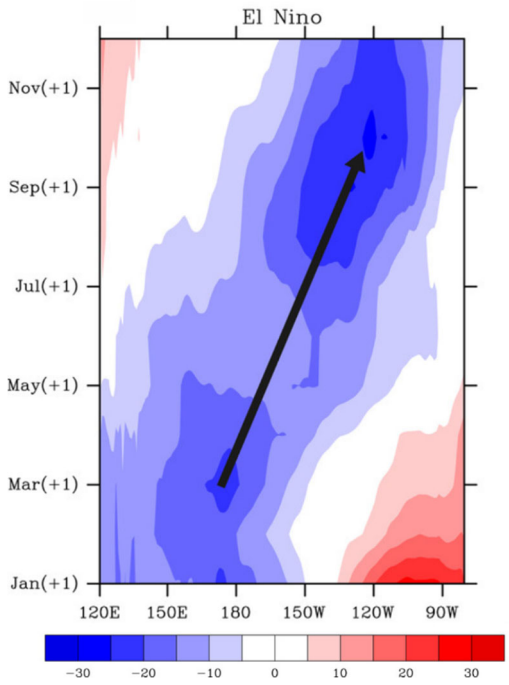

Figure 6.4: Composite time evolution of thermocline depth during an El Niño event. Evolution is from January (bottom) to November (top). Deeper thermoclines are indicated by blue.

The time evolution of ENSO is best illustrated by time series of various ENSO indices, which are based in whole or in part on equatorial sea surface temperature anomalies. One such index spanning the period 1980-2020 is reproduced in Figure 6.5. This multivariate index is the leading combined empirical orthogonal function of five different variables: sea level pressure, sea surface temperature, zonal and meridional components of the surface wind, and outgoing longwave radiation, over the tropical Pacific basin (30°S-30°N and 100°E-70°W). Positive values are associated with El Niño events. Exceptionally strong El Niños are evident in 1983, 1997 and 2016. The events occur irregularly every 2-7 years or so.

While not obvious in Figure 6.5, the evolution of El Niño events is strongly tied to the seasonal cycle. El Niño and La Niña episodes typically last 9-12 months. They both tend to develop during the Boreal spring (March-June), reach peak intensity during the late autumn or winter (November-February), and then weaken during the following Boreal spring or early summer (March-June).

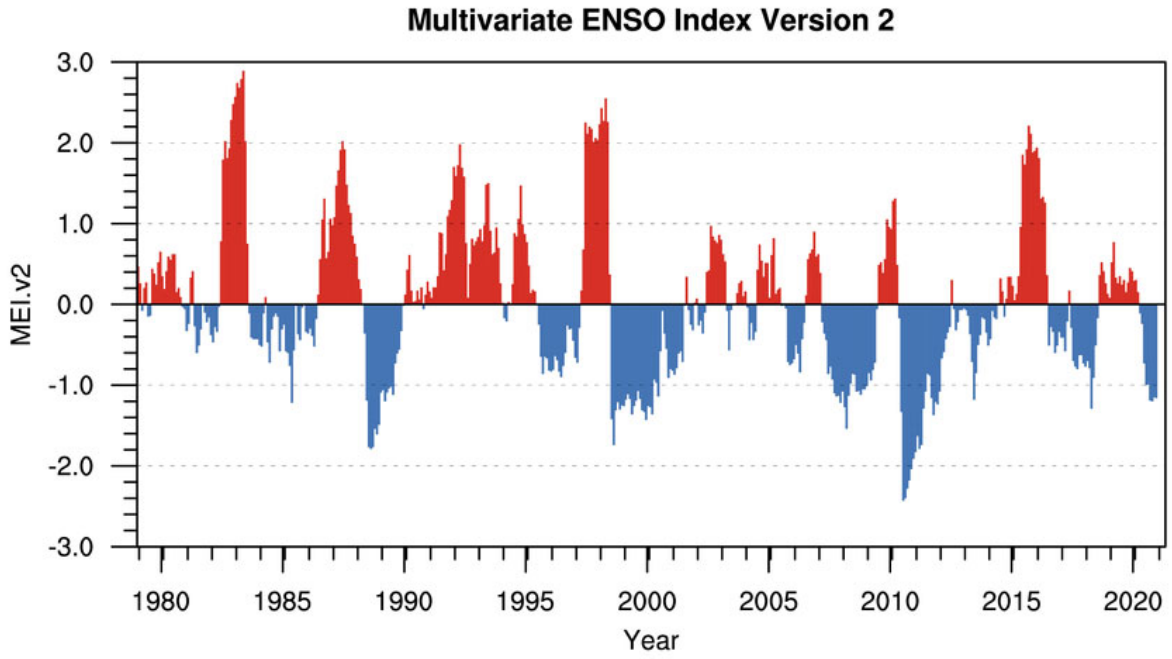

Figure 6.5: Evolution of a multivariate ENSO index from 1980 to 2020. Positive values are associated with El Niño events.

While ENSO is usually measured and characterized in terms of sea surface temperature anomalies in the equatorial Pacific, it is associated with strong short-term climate perturbations around the world. Some of these effects are summarize in Figure 6.6. Some of these weather patterns depend on the particular character of El Niño events, especially whether the positive sea surface temperature anomalies peak in the central versus eastern Pacific (Figure 6.1). Besides some of the characteristics illustrated in Figure 6.6, ENSO strongly modulates tropical cyclone activity in many regions; for example, El Niño tends to suppress North Atlantic tropical cyclone activity, which, conversely, is enhanced during La Niña conditions.

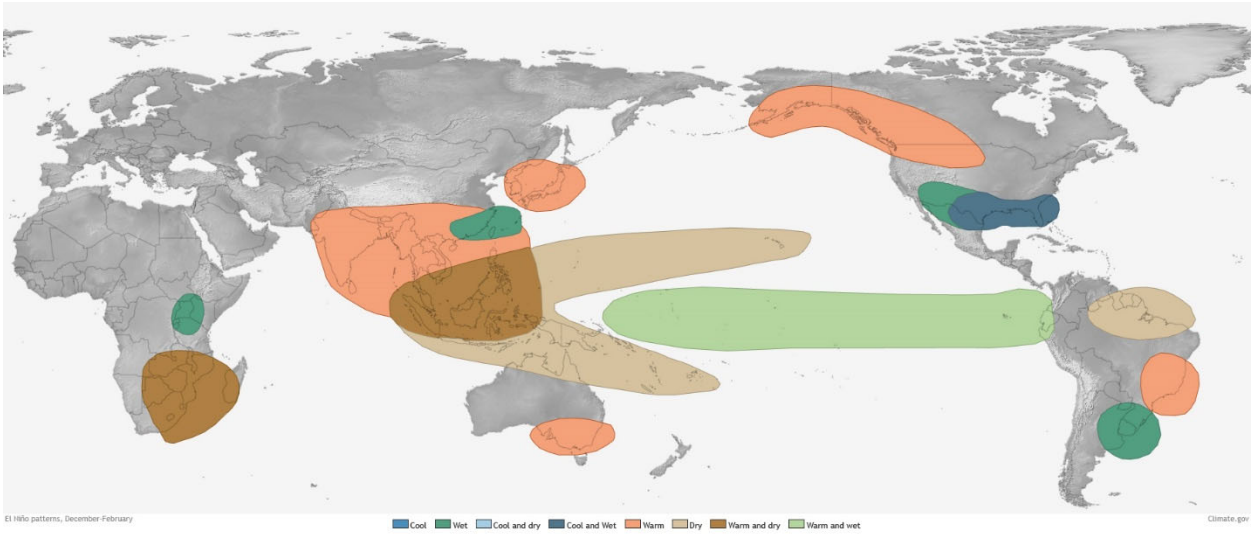

Figure 6.6: Short term climate variations during Boreal winter, associated with El Niño events. Light brown: dry conditions; lime green: warm and wet, ochre: warm, medium green: wet; dark brown: warm and dry, blue-green: cool and wet.

As has already been mentioned, ENSO has profound effects on marine life and is accompanied by strong shifts in everything from microbial populations to fish and seabirds. The very strong El Niño event of 1982-1983 led to large coral mortality in the tropical EASTERN Pacific. Thus, in addition to the inherent intellectual interest in ENSO, it has serious consequences for biological activity and human society.

6.2 Oscillations of the equatorial ocean

The physics of ENSO involve the interaction of the tropical atmosphere and ocean, both of which support a rich spectrum of wave modes. In general, the atmospheric waves are fast compared to their oceanic counterparts, which introduces some interesting subtleties in the interactions between the two media. We begin with discussion of linear wave modes on a resting equatorial ocean, continuing to treat it, to a first approximation, as a two-fluid system with an inert deep ocean superimposed by a less dense layer, treating the system using the shallow water approximation as in section 5.4.1. The shallow-water equations are phrased on an "equatorial $\beta-$plane", linearizing the sinusoidal dependence of the Coriolis parameter about its vanishing value at the equator: $f \simeq \beta y,$ where y is the distance north of the equator. These equations are

$$\frac{du}{dt} = -g' \frac{\partial h}{\partial x} + \beta y v + \frac{\tau_x}{h}, \tag{6.1}$$

$$\frac{dv}{dt} = -g' \frac{\partial h}{\partial y} - \beta y u + \frac{\tau_y}{h}, \tag{6.2}$$

$$\frac{dh}{dt} + h\left(\frac{\partial u}{\partial x} + \frac{\partial v}{\partial y}\right) = 0, \tag{6.3}$$

where, as before, u and v are the zonal and meridional velocities, h is the fluid depth, g' is the reduce gravitational acceleration, given by (5.59), and τ_x and τ_y are the zonal and meridional surface wind stresses.

We begin by linearizing these three equations about a resting state in which the wind stresses and velocities are zero and the fluid depth is D. Denoting perturbations to this state with primes, we replace the variables with

$$\begin{aligned} u &\to u', \\ v &\to v', \\ \tau_x &\to \tau_x' \\ \tau_y &\to \tau_y' \\ h &\to D + h'. \end{aligned} \tag{6.4}$$

Substituting these into (6.1) – (6.3) and dropping quantities that are quadratic in the prime variables (but remember that the prime modifying g means something else) gives

$$\frac{\partial u'}{\partial t} = -g'\frac{\partial h'}{\partial x} + \beta y v' + \frac{\tau_x'}{D}, \tag{6.5}$$

$$\frac{\partial v'}{\partial t} = -g'\frac{\partial h'}{\partial y} - \beta y u' + \frac{\tau_y'}{D}, \tag{6.6}$$

and

$$\frac{\partial h'}{\partial t} + D\left(\frac{\partial u'}{\partial x} + \frac{\partial v'}{\partial y}\right) = 0. \tag{6.7}$$

First consider the case where there is no surface wind stress $(\tau = 0)$. In that case, there is no forcing of this system, but it does admit neutral, oscillatory modes. Of these, let's first consider a special solution to (6.5) – (6.7) for which $v' = 0$ everywhere. In that case, we can see that (6.5) and (6.7) constitute a closed system, while (6.6) restricts the meridional variation of the mode.

Taking $\tau = 0$ and eliminating u' between (6.5) and (6.7) yields

$$\frac{\partial^2 h'}{\partial t^2} - g' D\frac{\partial^2 h'}{\partial x^2} = 0. \tag{6.8}$$

This is clearly a wave equation that admits separable solutions of the form

$$h' = G(y)F(x \pm ct), \tag{6.9}$$

where $c \equiv \sqrt{g'D}$, F is any reasonably behaved function, and $G(y)$ is a function of y that we will determine using (6.6). Substituting (6.9) into (6.6) with $v' = \tau_y' = 0$ gives an equation for $G(y)$:

$$\frac{1}{G}\frac{dG}{dy} = \pm\frac{\beta}{c}y, \tag{6.10}$$

whose solution is

$$G = Ae^{\pm\frac{\beta}{2c}y^2}, \tag{6.11}$$

where A is an arbitrary integration constant. Here, as a boundary conditions, we must insist that the solution be well behaved as $y \to \pm\infty$, so we must take the negative choice in (6.11), which also means we must take the negative root in 6.9. Thus we have as a viable solution

$$h' = Ae^{\frac{-\beta}{2c}y^2}F\left(x-ct\right), \tag{6.12}$$

with $c = \sqrt{g'D}$ with c positive and F any reasonably well behaved function. This solution describes eastward-propagating, non-dispersive waves that decay exponentially away from the equator on a decay scale L_y given by

$$L_y \equiv \sqrt{\frac{2g'D}{c\beta}} = \sqrt{\frac{2c}{\beta}}. \tag{6.13}$$

This scale is called the *equatorial deformation radius*. Taking $g' = 0.06\ ms^{-2}$ and $D = 100\,m$ (see Figure 5.53), the eastward propagation speed c is about $2.5\ ms^{-1}$ and the equatorial deformation radius is about $650\,km$.

This special solution to (6.5) – (6.7) describes phenomena known as *equatorially trapped Kelvin waves*, named after William Thomson, Lord Kelvin (Thomson, 1880). These are the main means by which adjustments to localized forcing are propagated eastward in the equatorial ocean[1]. From (6.5) or (6.7) it is clear that the layer depth perturbations in zonal velocity perturbations are out of phase in these neutral waves, with positive depth perturbations associated with negative zonal velocity. The structure of an equatorial Kelvin wave is shown in Figure 6.7; here a sinusoidal zonal structure has been assumed.

[1] The waves described here are more precisely defined as first baroclinic mode waves. There are also barotropic Kelvin waves that fill the depth of the ocean and for which the restoring force is gravity acting on perturbations of the sea surface elevation. These have a phase speed of about $150\ ms^{-1}$, and while they can be excited by earthquakes, they are not important in ENSO dynamics.

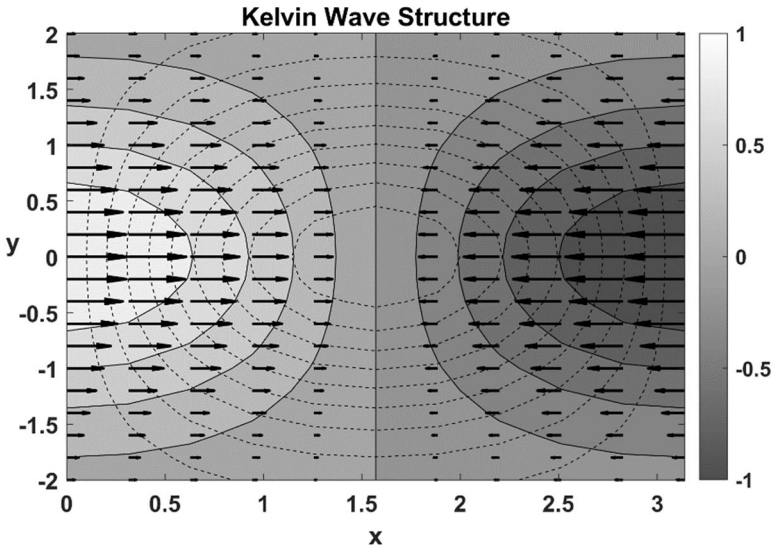

Figure 6.7: Structure of an equatorial Kelvin wave. All quantities are nondimensional, with the x axis in radians, spanning one-half wavelength. Shading shows thermocline depth perturbations, arrows show zonal velocity, and dashed contours show downwelling velocity. The wave is propagating eastward.

The general solutions to the unforced versions of (6.5) – (6.7) were first described by Taro Matsuno (Matsuno, 1966). Since the coefficients are independent of time and longitude, there is a class of solutions that are oscillatory in x and t and which we insist be well behaved (not blow up) when $y \to \pm\infty$. Thus we look for viable solutions of (6.5) – (6.7) with $\tau' = 0$ of the form

$$[u', v', h'] \to [U(y), V(y), H(y)] e^{ikx - i\omega t}, \tag{6.14}$$

where k is a zonal wavenumber and ω is the wave frequency. If we substitute (6.14) into (6.5) – (6.7) and eliminate $U(y)$ and $H(y)$ in favor of $V(y)$, we obtain a second-order ordinary differential equation:

$$\frac{d^2V}{dy^2} + V\left[\frac{\omega^2}{c^2} - k^2 - \frac{\beta k}{\omega} - \frac{\beta^2 y^2}{c^2}\right] = 0, \tag{6.15}$$

with $c \equiv \sqrt{g'D}$, as before. It is helpful to write this more simply by nondimensionalizing the frequency, wavenumber, and y according to

$$\begin{aligned} \omega &\to \sqrt{c\beta}\,\omega, \\ k &\to \sqrt{\beta/c}\,k, \\ y &\to \sqrt{c/\beta}\,y, \end{aligned} \tag{6.16}$$

whereupon (6.15) becomes

$$\frac{d^2V}{dy^2}+V\left[\omega^2-k^2-\frac{k}{\omega}-y^2\right]=0, \tag{6.17}$$

This is Schrödinger's equation for a quantum harmonic oscillator, which has well behaved solutions only if the wave frequency takes on certain discrete values given by the solution of

$$\omega^2-k^2-\frac{k}{\omega}=(2n+1), \tag{6.18}$$

where $n=0,1,2....$ and the eigenfunctions are parabolic cylinder functions:

$$V\sim e^{-\frac{1}{2}y^2}\left[1,2y\,,4y^2-2,...\right] \tag{6.19}$$

where the polynomial in brackets are the first three Hermite polynomials[2]. The n^{th} Hermite polynomial corresponds to the integer n in the dispersion relation (6.16).

Note that (6.18) is invariant to changing the signs of both ω and k as is the phase speed, ω/k. By convention, we allow negative values of k but not ω.

For $n=0$ The cubic dispersion relation (6.18) can be factored:

$$(\omega+k)\left[\omega^2-\omega k-1\right]=0. \tag{6.20}$$

The particular $\omega=-k$ is unphysical and corresponds to solutions that are not well behaved for large y, leaving two roots:

$$\omega=\frac{1}{2}\left[k\pm\sqrt{k^2+4}\right]. \tag{6.21}$$

Since by convention we allow negative k (corresponding to westward phase propagation) but not negative ω, we select the positive root of (6.21).

In the limit of large negative k, (6.21) becomes $\lim_{k\to-\infty}\omega=\frac{1}{|k|}$, or re-dimensionalizing using (6.16), $\omega\sim\frac{\beta}{|k|}$. In this limit, the solutions are equatorially trapped, westward propagating Rossby waves (remember that this is a limit in which k is negative). When k is large and positive, (6.21) becomes $\lim_{k\to\infty}\omega=k$, or in dimensional terms, $\omega=ck$. This is the dispersion relation for Kelvin waves, in which buoyancy is restoring force. In between these limits, the index of refraction depends on both c and β, and so these $n=0$ solutions are called *mixed*

[2] A general expression for the n^{th} Hermite polynomial is $H_n(y)=(-1)^n e^{y^2}\frac{d^n}{dy^n}e^{-y^2}$.

Rossby-gravity waves, or alternatively *Yanai waves*, named after the tropical meteorologist Michio Yanai (Yanai and Maruyama, 1966) who discovered them in stratospheric data.

For $n > 0$ solutions to (6.20) fall into two classes: High frequency, equatorially trapped internal gravity-inertia waves called *Poincare waves*, and low frequency, strictly-westward propagating Rossby–like waves. For the low-frequency modes, we ignore the first term in (6.18) and re-dimensionalize the result using (6.16) to get

$$\omega \simeq \frac{-k\beta}{k^2 + (2n+1)\frac{\beta}{c}}. \tag{6.22}$$

In the longwave limit, they behave like westward-propagating inertia-gravity waves, but in the high negative (westward) zonal wavenumber limit they are equatorially trapped Rossby waves. The phase speeds of these low frequency modes are always negative but their group velocity can be positive for sufficiently short waves.

In the high frequency limit we ignore the third term in (6.18) and in that case, the dimensional solution is

$$\omega^2 \simeq c^2k^2 + (2n+1)\beta c. \tag{6.23}$$

These are the eastward and westward propagating Poincare waves.

The full dispersion diagram illustrating the solutions to (6.18) are shown in Figure 6.8. Note that the Poincare waves and the Yanai wave have nonzero frequency when $k = 0,$ indicating zonally symmetric standing oscillations.

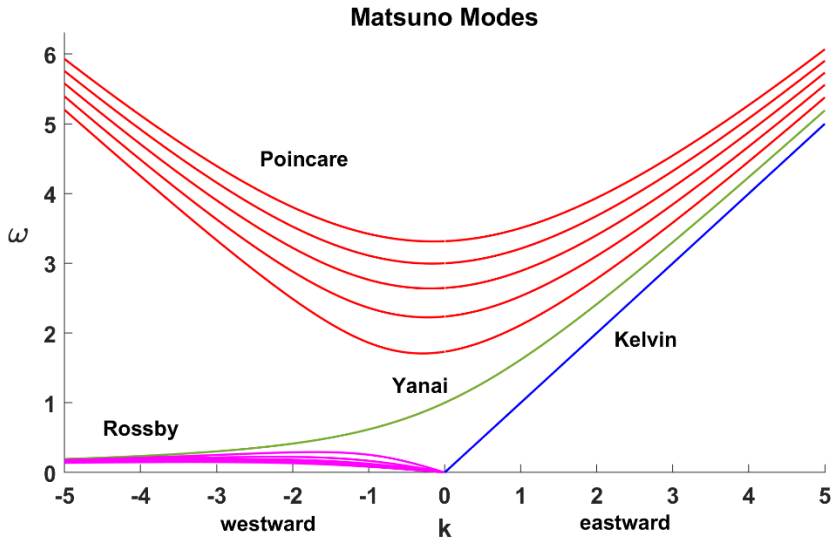

Figure 6.8: Nondimensional frequency as a function of nondimensional zonal wavenumber; solutions to (6.18). The Kelvin wave is shown in blue, the Yanai wave in green, Equatorial Rossby waves in magenta, and Poincare waves in red.

An example of an eigenfunction, for the $k = -1$ Yanai wave, is shown in Figure 6.9. This mode has a relatively complex structure, with vanishing depth, zonal velocity and vertical velocity at the equator, and maximum values at about one equatorial deformation radius north and south of the equator. Cyclonic and anticyclonic gyres alternate, with gyre centers at the equator. The vertical velocity is in quadrature with the depth perturbations. The interested reader can plot eigenfunctions of other modes using the script *Matsuno.m* available at the book's website.

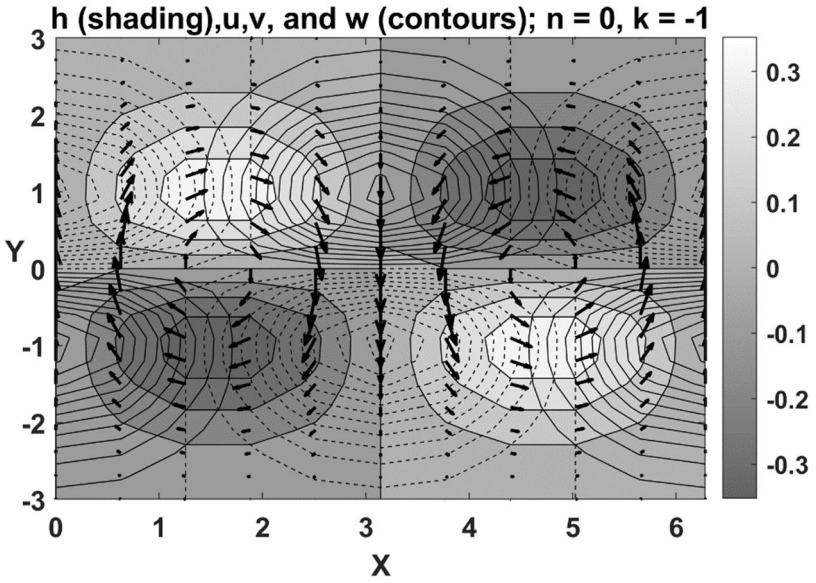

Figure 6.9: Eigenfunction for the Yanai wave (n=0) with k=-1. The shading shows the nondimensional fluid depth perturbation, the arrows shows the horizontal perturbation velocity vectors, and the thin black contours show the upward motion, with dashed contours indicating negative values.

Note that if $c = 2.5\ ms^{-1}$, and using the equatorial value of β, the dimensional wavelength associated with wavenumber 1 is about 2,800 km and a nondimensional frequency of 1 corresponds to a period of about 14 days. Consulting Figure 6.8 and noting that El Niño evolves over months, the main kinds of waves involved are low frequency Rossby and Kelvin waves. We will return to the role of these waves in ENSO evolution in section 6.4, but on our way to thinking about the fully coupled problem we must first look at the atmospheric response to surface anomalies on the scale of the equatorial Pacific.

6.3 The atmospheric response to large-scale equatorial surface flux anomalies

ENSO evolves slowly enough that, to a first approximation, the atmospheric response to ENSO-related sea surface temperature anomalies can be considered steady on atmospheric dynamical time scales. On the other hand, the very large spatial scales and slow time scales of ENSO imply that the weak-temperature -gradient approximation cannot be applied here as we have, for example, in considering the Walker Circulation on the equator, as we did in Chapter 5. We must include the effect of Coriolis accelerations, but we did in examining equatorial ocean

dynamics, we will approximate its variation as linear, continuing to use the equatorial β-plane approximation.

The principal simplifying assumption we will make about the atmosphere is that in regions experiencing deep convection, the lapse rate of temperature is moist adiabatic. As noted in Chapter 3, this is well satisfied, especially if one assumes reversible moist adiabatic ascent from the top of the subcloud layer. But here we will ignore the direct effects of water substance on density and assume that the saturation entropy is constant with altitude above cloud base, and equal to the actual moist entropy of air in the subcloud layer. As a reminder, the saturation entropy is given by

$$s^* = c_p \ln\left(T/T_0\right) - R_d \ln\left(p/p_0\right) + \frac{L_v q^*}{T}, \tag{6.24}$$

where T_0 and p_0 are reference temperature and pressure, respectively. We assume that while s^* varies in horizontal space and in time, it is always uniform above cloud base in the troposphere.

6.3.1 Dynamics

Now consider linear perturbations to a resting tropical atmosphere in RCE, denoting departures from the resting state with primes. First, we write the hydrostatic equation in pressure coordinates as

$$\frac{\partial \phi'}{\partial p} = -\alpha', \tag{6.25}$$

where, as usual, ϕ is the geopotential and α is the specific volume.

Using the chain rule and one of Maxwell's relations (Chapter 2), this can be written

$$\alpha' = \left(\frac{\partial \alpha}{\partial s^*}\right)_p s^{*\prime} = \left(\frac{\partial T}{\partial p}\right)_{s^*} s^{*\prime}. \tag{6.26}$$

This shows that in a hydrostatic, most adiabatic atmosphere, specific volume perturbations are constrained to have moist adiabatic vertical profiles. Substituting (6.26) into (6.25) gives

$$\frac{\partial \phi'}{\partial p} = -\left(\frac{\partial T}{\partial p}\right)_{s^*} s^{*\prime}. \tag{6.27}$$

Because we are assuming that $s^{*\prime}$ is not a function of pressure, we can integrate (6.27) from the top of the subcloud layer to the tropopause to get

$$\phi' = \phi_{bt}'(x,y,t) + \left(\overline{T}(x,y,t) - T(p)\right) s^{*\prime}, \tag{6.28}$$

where we have divided the integration constant into two parts: a height-independent mean temperature, $\overline{T}$, that multiplies the perturbation saturation entropy, and a height-independent geopotential, ϕ_{bt}. The former is just the pressure-weighted mean temperature of the troposphere above cloud base, and the latter we call the barotropic component of the geopotential. Note from the definition of $\overline{T}$ that the pressure-mean geopotential perturbation consists only of its barotropic component. The second term on the right of (6.28) describes what has come to be called the *first baroclinic mode* of tropical dynamics.

The relation (6.28) is a very powerful constraint on the dynamics of deep convecting regimes. It filters all vertical modes except the barotropic and first baroclinic modes, and reduces the full primitive equations to a barotropic vorticity equation and equations that take the mathematical form of shallow water equations, as shown presently.

The hydrostatic horizontal momentum equations linearized about a state of rest on an equatorial best plane are

$$\frac{\partial u'}{\partial t} = -\frac{\partial \phi'}{\partial x} + \beta y v' + g\frac{\partial \tau_x'}{\partial p}, \tag{6.29}$$

and

$$\frac{\partial v'}{\partial t} = -\frac{\partial \phi'}{\partial y} - \beta y u' + g\frac{\partial \tau_y'}{\partial p}, \tag{6.30}$$

where τ_x and τ_y are the horizontal components of wind stress. We specialize these to the cloud layer by assuming that the stress terms vanish above the subcloud later, and by substituting (6.28) for the geopotential terms:

$$\frac{\partial u'}{\partial t} = -\frac{\partial \phi_{bt}'}{\partial x} - \left(\overline{T} - T\right)\frac{\partial s^{*\prime}}{\partial x} + \beta y v', \tag{6.31}$$

and

$$\frac{\partial v'}{\partial t} = -\frac{\partial \phi_{bt}'}{\partial y} - \left(\overline{T} - T\right)\frac{\partial s^{*\prime}}{\partial y} - \beta y u', \tag{6.32}$$

where $\overline{T}$ is now a constant representing the basic state, and T is a function of pressure only. Inspection of these two equations shows that the solutions for the horizontal velocities can be broken down the same way as geopotential, namely

$$(u', v') = (u_{bt}', v_{bt}') + \frac{\overline{T} - T}{\overline{T} - T_{PBL}}\left(u_{bc}', v_{bc}'\right), \tag{6.33}$$

where the subscript *bt* and *bc* refer to the barotropic and baroclinic components, respectively, and T_{PBL} is the base state temperature at the top of the subcloud layer. Note that the primed variables in (6.33) are functions of x, y, and t only; all the vertical structure is in the $\overline{T} - T$

term. Substitution of the forms (6.33) into (6.31) and (6.32) gives two pairs of equations for the baroclinic and barotropic components. The set for the baroclinic component is

$$\frac{\partial u_{bc}'}{\partial t} = -\left(\overline{T} - T_{PBL}\right)\frac{\partial s^{*\prime}}{\partial x} + \beta y v_{bc}', \tag{6.34}$$

and

$$\frac{\partial v_{bc}'}{\partial t} = -\left(\overline{T} - T_{PBL}\right)\frac{\partial s^{*\prime}}{\partial y} - \beta y u_{bc}'. \tag{6.35}$$

Clearly, we need an equation for the tropospheric temperature, as represented by $s^{*\prime}$ to close the baroclinic system. If this equation depends, among other things, on the barotropic component of the pressure and/or velocity, then we will also need to solve for the barotropic component even if our interest were to lie solely with the baroclinic component.

The equations for the barotropic component are decoupled from temperature:

$$\frac{\partial u_{bt}'}{\partial t} = -\frac{\partial \phi_{bt}'}{\partial x} + \beta y v_{bt}', \tag{6.36}$$

and

$$\frac{\partial v_{bt}'}{\partial t} = -\frac{\partial \phi_{bt}'}{\partial y} - \beta y u_{bt}'. \tag{6.37}$$

We can form a vorticity equation by eliminating ϕ_{bt}' from (6.36) and (6.37):

$$\frac{\partial}{\partial t}\left(\frac{\partial v_{bt}'}{\partial x} - \frac{\partial u_{bt}'}{\partial y}\right) = -\beta y\left(\frac{\partial u_{bt}'}{\partial x} + \frac{\partial v_{bt}'}{\partial y}\right) - \beta v_{bt}'. \tag{6.38}$$

Now we can write the full equation of mass continuity as

$$\frac{\partial \omega'}{\partial p} = -\left(\frac{\partial u'}{\partial x} + \frac{\partial v'}{\partial y}\right) = -\left(\frac{\partial u_{bt}'}{\partial x} + \frac{\partial v_{bt}'}{\partial y}\right) - \frac{\overline{T} - T}{\overline{T} - T_{PBL}}\left(\frac{\partial u_{bc}'}{\partial x} + \frac{\partial v_{bc}'}{\partial y}\right), \tag{6.39}$$

where we have substituted (6.33) breaking down the velocities into baroclinic and barotropic components. We next integrate (6.39) down from the tropopause to and arbitrary pressure p :

$$\omega' = \omega_t' - (p - p_t)\left(\frac{\partial u_{bt}'}{\partial x} + \frac{\partial v_{bt}'}{\partial y}\right) - J(T)\left(\frac{\partial u_{bc}'}{\partial x} + \frac{\partial v_{bc}'}{\partial y}\right), \tag{6.40}$$

where ω_t' is the value of ω' at the tropopause, whose pressure is p_t, and

$$J(T) \equiv \int_{p_t}^{p} \frac{\overline{T} - T}{\overline{T} - T_{PBL}} dp. \tag{6.41}$$

Evaluating (6.40) at the top of the subcloud layer gives

$$\omega'_{PBL} = \omega'_t - \Delta P\left(\frac{\partial u_{bt}'}{\partial x} + \frac{\partial v_{bt}'}{\partial y}\right), \tag{6.42}$$

where $\Delta P \equiv p_{PBL} - p_t$ is the pressure depth of the cloud layer. The last term in (6.40) vanishes because, by definition, $J(T)$ vanishes at the top of the subcloud layer.

Note that the barotropic vorticity equation (6.38) together with (6.42) constitutes a close system if both ω'_t and ω'_{PBL} are known. We have to determine these two variables by matching what is going on in the cloud layer with equations expressing the dynamics of the stratosphere above, and equations describing the behavior of the subcloud layer below. In particular, if our tropospheric system supports waves, such as Kelvin and Rossby waves, we would expect them to couple to some extent with wave modes in the stratosphere. The latter has to be treated as a continuously stratified fluid (as its name implies!) but open-ended at the top, so that we may (expect upward wave energy propagation. The leakage of wave energy from the troposphere may damp disturbances there; a point we shall return to in Chapter 7[3]. But for the very slowly evolving ENSO, leakage of energy into the stratosphere will be very small, and so for the present purpose we take the tropopause to act as a rigid lid:

$$\omega'_t = 0. \tag{6.43}$$

This leaves us with the problem if solving for the vertical motion at the top of the subcloud layer, ω'_{PBL}. To do so, we must write down linearized dynamics for the subcloud layer.

Over tropical oceans, the subcloud layer has nearly constant virtual potential temperature, and although the value of that temperature will vary with conditions, we will ignore these here and assume that the horizontal pressure gradients do not vary with depth within the layer, so that, in effect, the pressure gradient in the layer is imposed from above. We shall also assume that the frictional deceleration of the horizontal flow owing to surface friction is vertically uniform. These two conditions imply that the wind components themselves are independent of height. With these assumptions, the linearized momentum equations in the subcloud layer are

$$\frac{\partial u_{sc}'}{\partial t} = -\frac{\partial \phi_{bt}'}{\partial x} - \left(\overline{T} - T_{PBL}\right)\frac{\partial s^{*\prime}}{\partial x} + \beta y v_{sc}' + g\frac{\tau_{xs}'}{\Delta p}, \tag{6.44}$$

and

$$\frac{\partial v_{sc}'}{\partial t} = -\frac{\partial \phi_{bt}'}{\partial y} - \left(\overline{T} - T_{PBL}\right)\frac{\partial s^{*\prime}}{\partial y} - \beta y u_{sc}' + g\frac{\tau_{ys}'}{\Delta p}, \tag{6.45}$$

[3] If there is enough wind shear in the stratosphere, as for example accompanies the Quasi-Biennial Oscillation, there may be altitudes at which the background wind speed matches the speed of waves emanating from the troposphere. In that case, some wave energy may backscatter from these “critical levels” back down into the troposphere, providing a possible feedback of stratospheric dynamics on tropospheric waves.

where T_{PBL} is the base state temperature at the top of the subcloud layer, τ_{xs} and τ_{ys} are the surface wind stresses, Δp is the pressure depth of the subcloud layer, and the subscript sc refers to subcloud layer quantities. We can simplify these greatly by changing variables:

$$\begin{aligned} u_{sc}' &\rightarrow u_{bt}' + u_{bc}' + u_f', \\ v_{sc}' &\rightarrow v_{bt}' + v_{bc}' + v_f', \end{aligned} \tag{6.46}$$

where the new variables u_f' and v_f' represent departures of the subcloud layer velocities from the sum of the barotropic and baroclinic velocities just above the subcloud layer. Substitution of (6.46) into (6.44) and (6.45), and making use of (6.34) – (6.37) yields

$$\frac{\partial u_f'}{\partial t} = \beta y v_f' + g\frac{\tau_{xs}'}{\Delta p}, \tag{6.47}$$

and

$$\frac{\partial v_f'}{\partial t} = -\beta y u_f' + g\frac{\tau_{ys}'}{\Delta p}. \tag{6.48}$$

In the absence of any surface stresses, these describe pure inertial oscillations on an equatorial β plane and we assume that in this limit they vanish. But in general, surface stresses depend on the *full* surface winds, as expressed by (6.46), and so (6.47) and (6.48) couple the boundary layer winds to both the barotropic and baroclinic wind components. In particular, *surface friction fundamentally couples the barotropic and baroclinic components*.

Mass continuity applied to the boundary layer flow and integrated over the depth of the subcloud layer yields

$$\omega_{PBL}' = \Delta p\left(\frac{\partial u_f'}{\partial x} + \frac{\partial v_f'}{\partial y} + \frac{\partial u_{bt}'}{\partial x} + \frac{\partial v_{bt}'}{\partial y} + \frac{\partial u_{bc}'}{\partial x} + \frac{\partial v_{bc}'}{\partial y}\right). \tag{6.49}$$

If we eliminate ω_{PBL}' between (6.49) and (6.42), with $\omega_t' = 0,$ the result is

$$\left(\frac{\partial u_{bt}'}{\partial x} + \frac{\partial v_{bt}'}{\partial y}\right) = \frac{-\Delta p}{p_0 - p_t}\left(\frac{\partial u_f'}{\partial x} + \frac{\partial v_f'}{\partial y} + \frac{\partial u_{bc}'}{\partial x} + \frac{\partial v_{bc}'}{\partial y}\right). \tag{6.50}$$

This determines the barotropic divergence as a function of the divergence of the baroclinic and frictional components. This shows that the barotropic divergence is small compared to the sum of the baroclinic and frictional divergences. If we substitute (6.50) back into (6.49) we get

$$\omega_{PBL}' = \Delta p\left(1 - \frac{\Delta p}{p_0 - p_t}\right)\left(\frac{\partial u_f'}{\partial x} + \frac{\partial v_f'}{\partial y} + \frac{\partial u_{bc}'}{\partial x} + \frac{\partial v_{bc}'}{\partial y}\right). \tag{6.51}$$

Since boundary layers over tropical oceans are thing compared to the depth of the troposphere, the first bracketed term on the right side of (6.51) may be approximated by unity.

Now, except for needing a relation for the tropospheric temperature $s^{*\prime}$ together with the specification of surface wind stresses in terms of perturbation surface winds, the relations (6.34) – (6.35), (6.38), (6.47), (6.48), and (6.51) would constitute a closed system for the variables $u_{bc}', v_{bc}', u_f', v_f', \omega'_{PBL}$ and $s^{*\prime}$ (which, as well see presently, depends on ω'_{PBL}).

We next turn our attention to the thermodynamics that determine the perturbation saturation entropy, $s^{*\prime}$.

6.3.2 Thermodynamics

The basic thermodynamic framework we will use here is very similar to that developed in Chapter 3 but extended to non-steady conditions. Referring back to Figure 3.17, we can approximate the saturation entropy of the atmosphere by its value outside of deep convective clouds, since the latter cover a small fractional area and have density temperatures not very different from the clear air. The temperature tendency in the clear air reflects two competing processes: subsidence, which warms the column, and radiative cooling. For convenience, we repeat (3.56) here:

$$\frac{\partial h_d}{\partial t} = 0 = w_d \frac{d\overline{h}_d}{dz} - \alpha \dot{Q}_{cool} = w_d \mathbf{S} - \alpha \dot{Q}_{cool}, \tag{6.52}$$

where h_d is the dry static energy, $\mathbf{S}$ is the dry static stability along the base state moist adiabat, $\mathbf{S} \equiv d\overline{h}_d / dz$, and w_d is the vertical velocity between clouds, defined positive downward. We also repeat the equation for conservation of mass, (3.51):

$$w = \alpha \left(M_u - M_d \right) - w_d, \tag{6.53}$$

where w is the ensemble-averaged (large-scale) vertical velocity, α is specific volume, and M_u and M_d are the convective updraft and downdraft mass fluxes. In (6.53) we have neglected the fractional area σ covered by convection, compared to unity. We also repeat our formulation (3.58) relating convective downdraft mass flux to convective updraft mass flux through a precipitation efficiency, ϵ_p:

$$M_d = \left(1 - \epsilon_p\right) M_u. \tag{6.54}$$

Substituting (6.53) into (6.52) and using (6.54) gives

$$\frac{\partial h_d}{\partial t} = S\left(\alpha \epsilon_p M_u - w\right) - \alpha \dot{Q}_{cool}. \tag{6.55}$$

Air is warmed by convective updrafts, (through their forcing of environmental subsidence) and cooled by radiation and by adiabatic cooling associated with large-scale ascent.

Now both the dry static energy, h_d and the saturation entropy, s^*, are functions of pressure and temperature. Thus, on isobaric surfaces, there is a one-to-one relationship between fluctuations of the two quantities. First, we relate isobaric fluctuations of dry static energy to fluctuations of dry air entropy:

$$\delta h_d = T \delta s_d. \tag{6.56}$$

Now we relate isobaric fluctuations of specific volume to fluctuations of dry air entropy and to fluctuations of saturated entropy using (2.47) and (2.74), respectively:

$$\delta \alpha = \left(\frac{\partial T}{\partial p} \right)_{s_d} \delta s_d = \frac{1}{1 + r_t} \left(\frac{\partial T}{\partial p} \right)_{s^*} \delta s^*. \tag{6.57}$$

Neglecting the total water concentration r_t compared to unity, and using the definitions of dry and moist adiabatic lapse rates, Γ_d and Γ_m, we can write (6.57) as

$$\delta s^* = \frac{\Gamma_d}{\Gamma_m} \delta s_d. \tag{6.58}$$

Using (6.56) and (6.58), we can write the thermodynamic equation (6.55) as

$$T \frac{\Gamma_m}{\Gamma_d} \frac{\partial s^*}{\partial t} = \mathbf{S} \left(\alpha \epsilon_p M_u - w \right) - \alpha \dot{Q}_{cool}. \tag{6.59}$$

This will be the form of the thermodynamic equation we will use in deep convecting tropical atmospheres. Remember that we are continuing to assume that the temperature lapse rate is always moist adiabatic, and so s^* is constant with height. We choose to evaluate (6.59) just above the boundary layer in what follows.

As we did in Chapter 3, we will close for the convective updraft mass flux using the boundary layer quasi-equilibrium hypothesis, (3.53):

$$M_u = \rho w_{PBL} + \frac{F_h}{h_b - h_m}, \tag{6.60}$$

where recall that F_h is the surface enthalpy flux and h_b and h_m are the subcloud layer and free troposphere moist static energies. Substituting (6.60) into (6.59) evaluated just above the top of the boundary layer gives

$$\left(T \frac{\Gamma_m}{\Gamma_d} \right)_{PBL} \frac{\partial s^*}{\partial t} = \mathbf{S} \left(\frac{\alpha \epsilon_p F_h}{h_b - h_m} - \left(1 - \epsilon_p \right) w_{PBL} \right) - \left(\alpha \dot{Q}_{cool} \right)_{PBL}. \tag{6.61}$$

We note that in our base state of RCE, there is no time tendency of temperature and $w = 0$, so from (6.61)

$$S \epsilon_p \overline{\alpha F_h} = \left(\overline{h_b} - \overline{h_m} \right) \left(\overline{\alpha \dot{Q}_{cool}} \right)_{PBL}, \tag{6.62}$$

where the overbar represented the base state. If we make the further approximation that the base state (RCE) radiative cooling rate per unit mass is relatively constant with height in the troposphere (not usually a bad approximate; see Figure 3.21a), then overall energy balance requires that

$$\overline{\alpha F}_h = H\left(\overline{\alpha \dot{Q}_{cool}}\right)_{PBL}, \tag{6.63}$$

where $H = \frac{1}{g}\int_{p_t}^{p_0} \alpha dp$ is the scale height of the troposphere. We next linearize (6.61) around the basic RCE state, making use of (6.62) and (6.63) and ignoring fluctuations in precipitation efficiency and in the basic state stratification, $\mathbf{S}$, yielding

$$\left(T\frac{\Gamma_m}{\Gamma_d}\right)_{PBL}\frac{\partial s^{*\prime}}{\partial t} = \frac{\left(\alpha F_h{}'\right)}{H} - \frac{\overline{\alpha \dot{Q}_{cool}}}{\epsilon_p H \mathbf{S}}\left(h_b{}' - h_m{}'\right) - \mathbf{S}\left(1-\epsilon_p\right)w'_{PBL} - \left(\alpha \dot{Q}_{cool}\right)'_{PBL}. \tag{6.64}$$

Since we assume moist convective neutrality, fluctuations in subcloud layer moist entropy, $s_b{}'$ must equal fluctuations in the saturation entropy in the cloud layer, $s^{*\prime}$. Moreover, fluctuations of moist static energy, $h_b{}'$, are to a good approximation related to fluctuations of entropy by $h_b{}' \cong T s_b{}'$, so that we may write (6.64) as

$$\left(T\frac{\Gamma_m}{\Gamma_d}\right)_{PBL}\frac{\partial s^{*\prime}}{\partial t} = \frac{\left(\alpha F_h{}'\right)}{H} - \frac{\overline{\alpha \dot{Q}_{cool}}}{\epsilon_p H \mathbf{S}}\left(T s^{*\prime} - h_m{}'\right) - \mathbf{S}\left(1-\epsilon_p\right)w'_{PBL} - \left(\alpha \dot{Q}_{cool}\right)'_{PBL}. \tag{6.65}$$

This will be the linearized form of the tropospheric thermodynamic equation we will use here and in the next chapter, so it is worth describing the terms in some detail:

Term in (6.65)	Description
$\frac{\left(\alpha F_h{}'\right)}{H}$	Perturbations in the surface enthalpy flux lead, through deep convection, to heating or cooling of the cloud layer
$-\frac{\overline{\alpha \dot{Q}_{cool}}}{\epsilon_p H \mathbf{S}}\left(T s^{*\prime} - h_m{}'\right)$	A positive perturbation in boundary entropy, also proportional to $s^{*\prime}$, reduces the boundary layer quasi-equilibrium convective mass flux, cooling the troposphere. Likewise, a positive perturbation in mid-tropospheric moist static energy increases the mass flux, warming the troposphere.
$-\mathbf{S}\left(1-\epsilon_p\right)w'_{PBL}$	$\mathbf{S}\left(1-\epsilon_p\right)$ is the effective stratification of a moist convecting atmosphere. It is the dry stratification modified by moist convection according to how efficiently the convection precipitates.
$-\left(\alpha \dot{Q}_{cool}\right)'_{PBL}$	Perturbations in the radiative cooling rate directly cause change in tropospheric temperature.

Aside from needing to specify the perturbation surface fluxes and radiative cooling in terms of known variables, we also need an expression for the perturbation moist static energy of the cloud layer, and for that we turn to (3.64):

$$\frac{\partial h_m}{\partial t} = -\left\langle \mathbf{V}_h \bullet \nabla h \right\rangle - G w_{PBL} - \left\langle \alpha \dot{Q}_{cool} \right\rangle + \frac{g}{p_0 - p_t} F_h, \tag{6.66}$$

where recall that the angle brackets denote averaging over the troposphere, and that G is the gross moist stability. Linearizing this about the RCE state gives

$$\frac{\partial h_m'}{\partial t} = -G w'_{PBL} - \left\langle \alpha \dot{Q}_{cool} \right\rangle' + \frac{g}{p_0 - p_t} F_h'. \tag{6.67}$$

We represent surface enthalpy fluxes in terms of the aerodynamic flux formula (3.28) assuming neutral stability of the surface layer:

$$\alpha F_h = C_k \, | \mathbf{V}_s | \left(h_0^* - h_b \right), \tag{6.68}$$

where C_k is a nondimensional surface exchange coefficient, $| \mathbf{V}_s |$ is the surface wind speed, and h_0^* is the saturation moist static energy at sea surface temperature. In linearizing this about the RCE state, we assume that, in keeping with average conditions in the tropics, there is background easterly surface wind. In that case, the perturbation enthalpy flux is given by

$$\alpha F_h' = C_k \, | \bar{U} | \left(h_0^{*\prime} - h_b' \right) - C_k u_{sc}' \left(\overline{h_0^*} - \overline{h_b} \right), \tag{6.69}$$

where $| \bar{U} |$ is the magnitude of the background easterlies and u_{sc}' is the perturbation background zonal flow in the subcloud layer. The first term on the right side of (6.69) represents the effect of perturbations in sea surface temperature and boundary layer moist static energy on surface fluxes, while the second term indicates that easterly wind perturbations will, by adding to the background easterlies, enhance the surface enthalpy flux.

Aside from the radiative cooling perturbations, we now have a closed linear system consisting of (6.34), (6.35), (6.47), (6.48), (6.51), (6.65), (6.67) and (6.69). This is quite a notationally unwieldy system, but we can make it less cumbersome both by introducing some further small approximations and by nondimensionalizing the dependent and independent variables.

First, as indicated by (6.50) and (6.38), the barotropic velocities will be much smaller than the baroclinic and frictional components and we hereafter neglect them. We also approximate the first term in brackets in (6.51) as unity and use the hydrostatic equation to re-express it in terms of the vertical velocity at the top of the boundary layer:

$$w_{PBL}' \cong -d \left(\frac{\partial u_f'}{\partial x} + \frac{\partial v_f'}{\partial y} + \frac{\partial u_{bc}'}{\partial x} + \frac{\partial v_{bc}'}{\partial y} \right), \tag{6.70}$$

where d is the physical depth of the subcloud layer.

In equations (6.47) and (6.48) we represent the surface stress terms using neutral aerodynamic flux formulae, linearized around an easterly zonal mean wind to arrive at

$$\frac{\partial u_f{}'}{\partial t} = \beta y v_f{}' - \frac{2C_d\,|\bar{U}|}{d}\left(u_f{}' + u'_{bc}\right), \tag{6.71}$$

and

$$\frac{\partial v_f{}'}{\partial t} = -\beta y u_f{}' - \frac{C_d\,|\bar{U}|}{d}\left(v_f{}' + v'_{bc}\right). \tag{6.72}$$

The factor of 2 in the drag term in (6.71) results because perturbations in the zonal wind also contribute linearly to the net surface wind speed.

By adding equations (6.34) and (6.35) to (6.71) and (6.72), we notice that now the frictional and baroclinic velocities only appear in combination, so we can replace their sum by a single new variable.

In (6.67) we approximate the vertically averaged perturbation radiative cooling, $\left\langle \alpha \dot{Q}_{cool} \right\rangle'$, by its value just above the top of the subcloud layer, $\left(\alpha \dot{Q}_{cool}\right)'_{PBL}$.

Finally, we replace the dimensional independent and dependent variables by nondimensional counterparts as follows:

$$\begin{aligned}
&x \to ax, \qquad y \to L_y y, \qquad t \to \frac{a}{\beta L_y{}^2} t, \\
&u'_{bc} + u'_f \to \frac{aC_k\,|\bar{U}|}{H} u, \\
&v'_{bc} + v'_f \to \frac{L_y C_k\,|\bar{U}|}{H} v, \\
&w'_{PBL} \to \frac{dC_k\,|\bar{U}|}{H} w, \\
&\left(s^{*\prime}, s_0{}^{*\prime}\right) \to \frac{\beta L_y{}^2}{T_{PBL} - \bar{T}} \frac{aC_k\,|\bar{U}|}{H} \left(s, s_0\right), \\
&h'_m \to \frac{\epsilon_p \left(1-\epsilon_p\right) \mathbf{S}^2 H d}{\overline{h_0{}^*} - \overline{h^*}} h_m, \\
&\left(\alpha \dot{Q}_{cool}\right)'_{PBL} \to \frac{C_k\,|\bar{U}|\left(1-\epsilon_p\right)\mathbf{S}d}{H} Q,
\end{aligned} \tag{6.73}$$

where

$$L_y \equiv \left(\frac{\Gamma_d}{\Gamma_m} \frac{T_{PBL} - \bar{T}}{T_{PBL}} \frac{\mathbf{S}d\left(1-\epsilon_p\right)}{\beta^2} \right)^{\frac{1}{4}}. \tag{6.74}$$

With these substitutions, the linear perturbation equations take the form

$$\frac{\partial u}{\partial t} = \frac{\partial s}{\partial x} + yv - 2Du, \tag{6.75}$$

$$\frac{\partial v}{\partial t} = \delta\left(\frac{\partial s}{\partial y} - yu\right) - Dv, \tag{6.76}$$

$$w = -\left(\frac{\partial u}{\partial x} + \frac{\partial v}{\partial y}\right), \tag{6.77}$$

$$\frac{\partial s}{\partial t} = \chi\left(s_0 - s\right) - \chi_2 s - \alpha u - w + h_m - Q, \tag{6.78}$$

and

$$\gamma\frac{\partial h_m}{\partial t} = \chi\left(s_0 - s\right) - \alpha u - G_m w - Q, \tag{6.79}$$

where the nondimensional coefficients are defined as follows:

$$\begin{aligned}
\delta &\equiv \frac{a^2}{L_y{}^2}, \\
D &\equiv \frac{C_k\,|\bar{U}\,|\,a}{d\beta L_y{}^2}, \\
\chi &\equiv \frac{C_k\,|\bar{U}\,|\,a}{H}\sqrt{\frac{T_{PBL}}{T_{PBL}-\bar{T}}\frac{\Gamma_d}{\Gamma_m}\frac{1}{\mathbf{S}d\left(1-\epsilon_p\right)}}, \\
\chi_2 &\equiv \chi\left(\frac{\overline{h^*{}_0} - \overline{h^*}}{\epsilon_p \mathbf{S}H}\right), \\
\alpha &\equiv \frac{C_k a}{H}\frac{\overline{h^*{}_0} - \overline{h^*}}{\mathbf{S}d\left(1-\epsilon_p\right)}, \\
G_m &\equiv \frac{G}{\mathbf{S}\left(1-\epsilon_p\right)}, \\
\gamma &\equiv \frac{\epsilon_p \mathbf{S}H^2\beta L_y{}^2}{C_k\,|\bar{U}\,|\,a\left(\overline{h^*{}_0} - \overline{h^*}\right)}.
\end{aligned} \tag{6.80}$$

The set (6.75)-(6.81) constitutes are model of linear perturbations to deep convecting regions on an equatorial $\beta-$plane. In the next section we will use these to estimate the response of the convecting equatorial atmosphere to sea surface temperature perturbations.

6.3.3 Tropical atmospheric response to slowly evolving sea surface temperature anomalies

ENSO evolves on time scales that are long compared to the atmospheric dynamic response to changing sea surface temperature. The time scale used in (6.73) to nondimensionalize time has a characteristic value of a few days, for example. Thus, we can look for the steady response to prescribed sea surface temperature anomalies (represented in (6.80) and (6.81) by the saturation entropy of the sea surface) by setting the time derivatives in (6.75) – (6.81) to zero. To make the solutions more analytically tractable, we will focus on solutions with no surface drag or radiative forcing by setting D and Q to zero:

$$\frac{\partial s}{\partial x} = -yv, \tag{6.81}$$

$$\frac{\partial s}{\partial y} = yu, \tag{6.82}$$

$$w = -\left(\frac{\partial u}{\partial x} + \frac{\partial v}{\partial y}\right), \tag{6.83}$$

$$\alpha u + G_m w + \chi s = \chi s_0. \tag{6.84}$$

This is a complete set, and (6.78) becomes a simply diagnostic relation for the mid-tropospheric moist static energy perturbation, h_m. Using cross-differentiation to eliminate all the variables in favor of the saturation entropy gives a single partial differential equation:

$$\tilde{\alpha} y \frac{\partial s}{\partial y} - \tilde{G} \frac{\partial s}{\partial x} + y^2 s = y^2 s_0, \tag{6.85}$$

where $\tilde{\alpha} \equiv \alpha / \chi$ and $\tilde{G} \equiv G_m / \chi$. The right side of (6.85) contains the sea surface saturation entropy distribution, which we will prescribe here. Remember that $\tilde{G}$ measures the gross moist stability, and $\tilde{\alpha}$ is a measure of the strength of the WISHE effect.

As an example, we represent the distribution of s_0 as the separable product of a function of y and a function of x, the latter of which we can take to be a discrete Fourier series, with the periodicity given by the circumference of the earth. Thus we specify

$$s_0 = \sum_{n=1:\infty} \mathrm{Re}\left[F_n(y) e^{inx}\right]. \tag{6.86}$$

Here n is the zonal wavenumber; remember that we have normalized x by the radius of the Earth. Likewise, we represent the solution as

$$s = \sum_{n=1:\infty} \mathrm{Re}\left[J_n(y)e^{inx}\right], \tag{6.87}$$

where, from substituting (6.87) into (6.86) the functions J_n must satisfy

$$\tilde{\alpha} y \frac{dJ_n}{dy} + \left(y^2 - \tilde{G}in\right)J_n = y^2 F_n(y). \tag{6.88}$$

Before proceeding, we note from the form of this equation that $J = 0$ at the equator, $y = 0$, thus there are no temperature perturbations on the equator. We also note that in the special case of no WISHE $(\alpha = 0)$, (6.88) has the simple solution

$$J_n = \frac{y^2 F_n(y)}{y^2 - \tilde{G}in}. \tag{6.89}$$

Otherwise, using variation of parameters, the general solution of (6.88) that satisfies the boundary condition at $y = 0$ is

$$J_n = \frac{1}{\tilde{\alpha}} y^{in\tilde{G}/\tilde{\alpha}} e^{-y^2/2\tilde{\alpha}} \int_0^y F_n(u) u^{1-in\tilde{G}/\tilde{\alpha}} e^{u^2/2\tilde{\alpha}} du. \tag{6.90}$$

Whether this function is well behaved for large y will depend on the function $F(y)$. The full solution for s is then found by substituting J into (6.87). Given the solution for s, we can then find u, v, and w from (6.81), (6.82), and (6.84).

Here we evaluate the integral in (6.89) numerically for a sea surface saturation entropy perturbation with a single sinusoidal zonal wavenumber of 2 and a distribution in y given by

$$F_n = e^{-1.5y^4}.$$

This distribution is quite flat near the equator but has sharp shoulders at higher latitudes, and is symmetric about the equator. The top row of Figure 6.10 shows the fields for the case in which $\tilde{G} = 0.8$ and $\alpha = 0$, for which the solution for s is given by (6.89). The vertical motion pattern in this case (left panel) strongly resembles the sea surface temperature distribution, but the temperature distribution peaks off the equator and more or less zonally in quadrature with the surface temperature. The wind distributions show cyclones and anticyclones around the warm and cold atmospheric temperature anomalies. It is important to note that the equatorial zonal wind is in quadrature with the sea surface temperature anomalies.

When the WISHE effect is added ($\alpha = 1$; second row in Figure 6.10), the whole pattern shifts eastward and extends to higher latitudes. In this case, the equatorial zonal winds have their maximum magnitudes near the peaks in the surface temperature distribution, with strong westerly surface winds over the warmest water. This is because the maximum surface enthalpy flux is shifted eastward toward the maximum surface easterly winds, where the net surface wind speed is maximum. With $\alpha = 1$, this has a strong effect on the surface enthalpy flux.

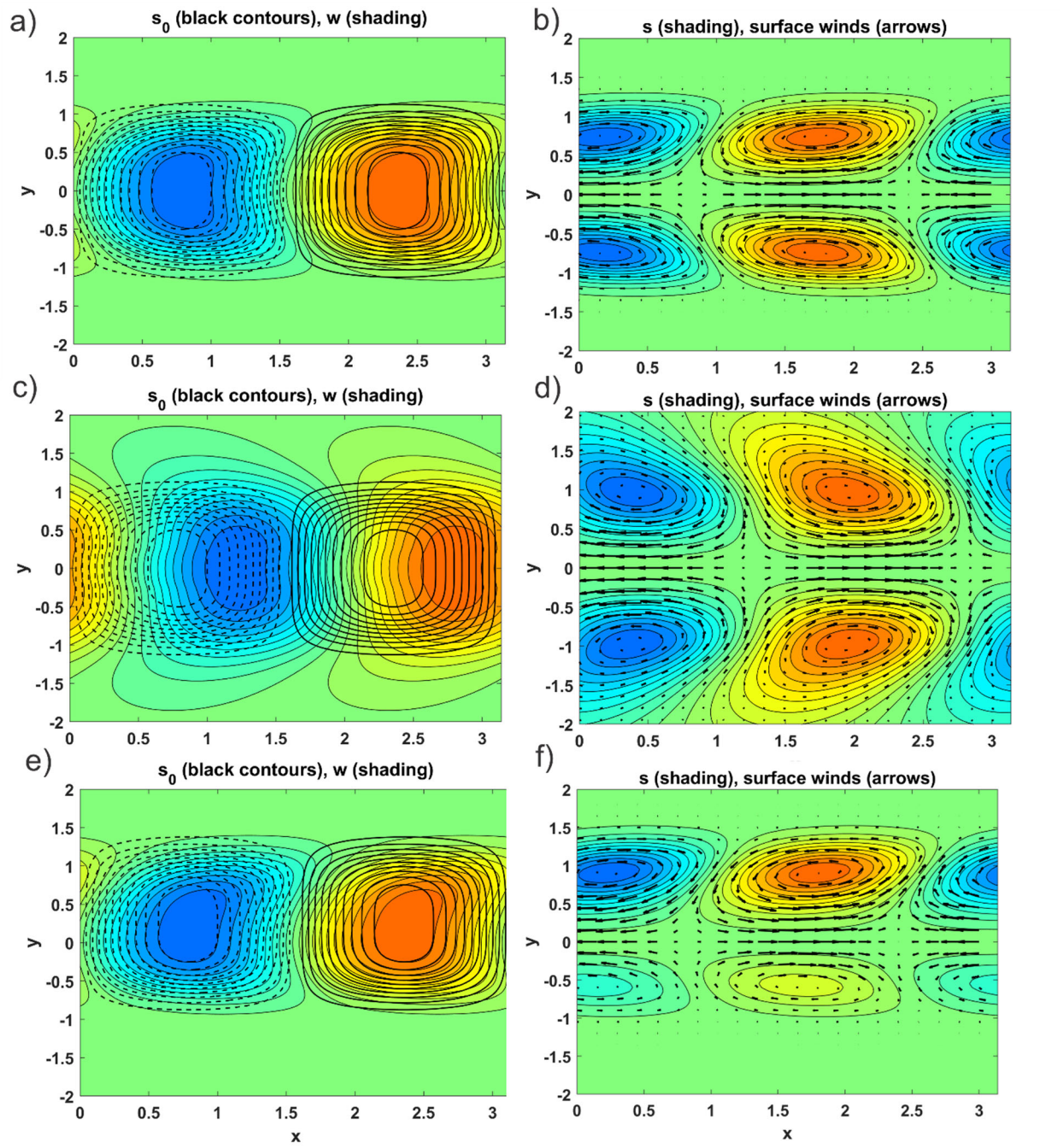

Figure 6.10: Steady, frictionless response of the equatorial atmosphere to sea surface saturation entropy anomalies as described in the text. In each row, the left-hand panel shows the specified distribution of s_0 *(black contours, with dashed showing negative values) and vertical velocity* w *(shading; warm colors positive); the left-hand panel shows saturation entropy* s *(shading) and horizontal winds (arrows). For all plots,* $\tilde{G}=0.8$ *and for the top and bottom rows,* $\alpha=0$ *while for the middle row* $\alpha=1$*. The third row is for conditions identical to the first except that the* s_0 *anomaly pattern has maximum amplitude at* $y=0.25$.

The last row in Figure 6.10 is for conditions identical to those used to construct the first row, except that the sea surface saturation enthalpy pattern has been shifted northward so as to have maximum amplitude at $y = 0.25$. Even this relatively small northward displacement dramatically shifts the temperature and horizontal winds response into the northern hemisphere, even though the vertical motion pattern is hardly affected.

The reader is encouraged to explore these solutions using the code *Gill.m*, which can be found on the course website.

One problem with this solution is that, when $D = 0$ and $\alpha > 0$, the basic state turns out to be absolutely unstable. For this reason, the solutions shown here must be regarded, at best, as the steady part of a time-evolving pattern. We will explore the linear instability of this system in detail in Chapter 7.

Gill (1980) found solutions for the system presented here for the case $\alpha = 0$ and for small values of D. He showed that the homogeneous solution can be expressed in terms of parabolic cylinder functions and found analytic solutions in the case where the forcing also has the form of the first or the second parabolic cylinder function. In both cases he sought solutions in which the forcing was confined to a limited range of x rather than being periodic in x as we have specified here.

Here we will solve the system (6.75) – (6.79), for the case $Q = 0,$ by numerically marching forward in time until a steady state is attained. Given today's computational speeds, this is quite fast and allows one the flexibility of specifying any reasonable distribution of the sea surface temperature. But here we continue to take the sea surface temperature and the forced solutions to be sinusoidal in $x,$ so as before we replace all the dependent variables by complex functions of y multiplied by e^{imx}. The code used to generate these solutions, *GillD.m*, is available on the course website.

Results for the same function of y as we used in the zero drag case are shown in Figure 6.11, which is in the same format as Figure 6.10, but also includes contours of the normalized moist static energy perturbation, for a fairly strongly damped case with $D = 0.5,$ $\alpha = 1,$ $G_m = 0.8,$ $\chi = 1,$ $\chi_2 = 0.5,$ and $\delta = 10.$ Surface drag strongly changes the solution. The vertical velocity, which was strongly shifted eastward from the sea surface entropy pattern in the zero drag case with WISHE, is shifted back to more nearly coincide with the sea surface entropy. Now there are large atmosphere temperature (saturation entropy) perturbations on the equator. One can also notice flow down the pressure gradient in the off-equator gyres. Recall that these are the sum of the baroclinic and frictional velocities; we could now solve the nondimensional equivalents of (6.71) and (6.72) for the frictional and baroclinic velocities separately. Note, however, that one or both of these would have a singularity at the equator which cancels in their sum.

Armed with knowledge of the basic response of the atmosphere to sea surface temperature anomalies, we are now in a position to tackle the coupled ENSO system.

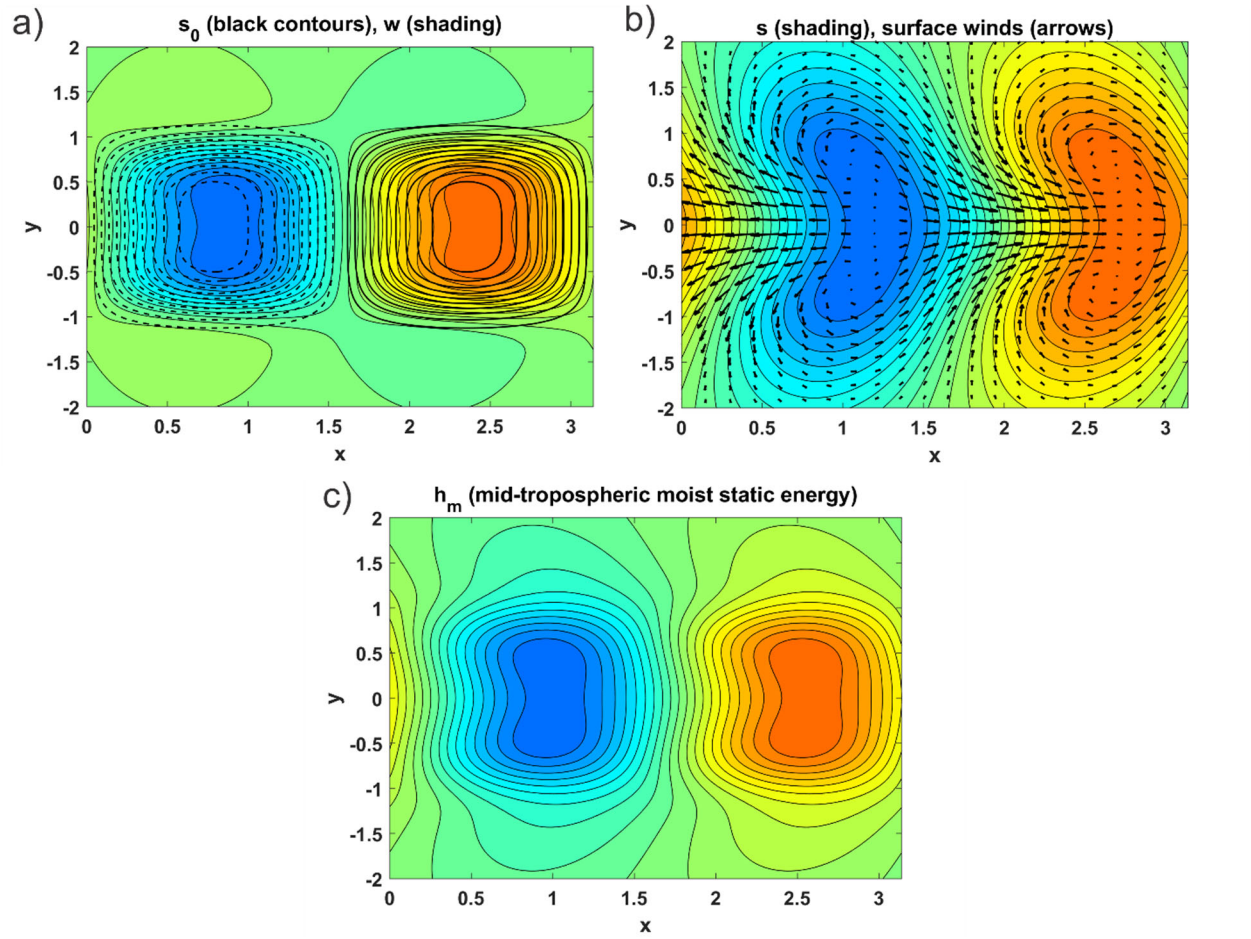

Figure 6.11: Panels a) and b) are the same as in Figure 6.10 but with surface drag included: D=0.5, α=1, G_m=0.8, χ=1, χ_2=0.5, *and* δ=10. *Panel c) is for the same parameters but shows the mid-level moist static energy perturbation.*

6.3.4 Dynamics of the fully coupled ENSO system

ENSO involves the complex interplay of equatorial waves in the ocean and atmosphere. The real system relies in part on partial reflection of equatorial ocean waves off continental boundaries as well as leakage of the some of the wave energy into coastally trapped waves. (See Federov and Brown (2009) for an excellent review of equatorial wave dynamics.) Here we provide a mostly qualitative overview of the fundamental dynamics of ENSO. The reader is referred to the review paper by Wang et al. (2017) for a more comprehensive overview.

At this writing, there are two views of ENSO dynamics. The first regards it as a fundamental instability of the Walker system resulting in growing and decaying oscillations. The second holds that the Walker system admits neutral and/or weakly damped modes that are stochastically excited by higher frequency disturbances of the equatorial region, such as the Madden-Julian Oscillation (see Chapter 7). In both cases, a mechanism first proposed by Bjerknes (1969) serves to amplify positive sea surface temperature perturbations in the central equatorial Pacific. With some small modifications, we describe this mechanism here.

Suppose a positive sea surface temperature anomaly is introduced into the central equatorial Pacific. Then, referring to either Figure 6.10 (middle row) or Figure 6.11, ascent will develop over the warm anomaly, but shifted eastward by the WISHE effect, given that the background surface flow in the Walker state is easterly. This will induce westerly surface wind anomalies to the west of the positive sea surface temperature anomaly, overlapping with the anomaly of the WISHE effect is present. Note that this is fully consistent with the observations summarized in Figure 6.2. The relaxation of the surface easterlies over and to the west of the warm ocean anomaly leaves the ocean pressure gradient, associated with the sloping thermocline in the Walker state, unbalanced, and so water begins to accelerate toward the east, advecting the warm pool water with it. This will both amplify the original anomaly and propagate it eastward, more or less at the speed of ocean Kelvin waves. Note that this is more likely to start in April, when, as part of the normal seasonal cycle of the central Pacific, the equatorial easterlies are weakest. (This may help explain why observed El Niño events are phase locked to the seasonal cycle.)

Once the eastern equatorial Pacific has warmed up and zonal gradients across the Pacific are weak, it is less clear how an El Niño event dissipates. (Indeed, there is paleoclimatological evidence that “permanent” El Niño states existed at certain times in the past, such as the Pliocene period (3-5 million years ago), but the evidence is controversial.) We point out here that if the equatorial winds averaged across the Pacific become westerly, as they are often observed to during El Niño episodes, the WISHE effect changes sign and the westerlies relax near the location of peak anomalous sea surface temperature. This is illustrated in Figure 6.12 which shows solutions for the same conditions as in Figure 6.11 (*a* and *b*) except that we assume background westerly winds $(\alpha = -1.5)$. The ascent is now shifted decidedly west of the warm sea surface temperature anomaly and the winds have also shifted westward. Easterly wind anomalies east of the warm ocean anomaly should enhance ocean upwelling there, acting to restore cold conditions. Note also the cyclonic gyres north and south of the position of the warm ocean anomaly. These also exist when mean easterlies are present (Figure 6.11) but are more zonally aligned with the ocean temperature with mean westerlies.

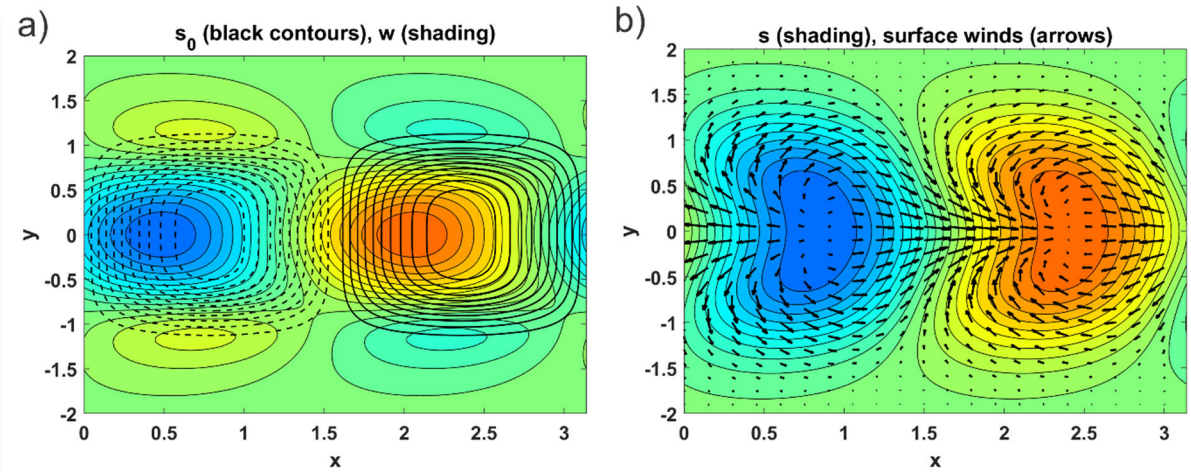

Figure 6.12: Same as Figure 6.11 a and b, except that $\alpha = -1.5$.

If we were to assume that the ENSO anomalies are slowly varying relative to the time scales of oceanic equatorial Kelvin and Rossby waves (not necessarily a very good assumption!) we could make certain deductions about the off-equatorial ocean currents from the steady forms of the shallow water equations, (6.5) and (6.6). Taking the derivative of (6.6) in x and subtracting from it the derivative of (6.5) in y gives

$$y\left(\frac{\partial u'}{\partial x}+\frac{\partial v'}{\partial y}\right)+v=\frac{1}{D\beta}\left(\frac{\partial \tau_y'}{\partial x}-\frac{\partial \tau_x'}{\partial y}\right), \tag{6.91}$$

where the velocities pertain to the ocean and D is here the thermocline depth. Recall that τ_x' and τ_y' are the meridional and zonal components of the surface wind stress per unit mass. But the steady form of (6.7) requires the divergence of the velocities to be zero, so the first term in (6.91) vanishes and we are left with

$$v=\frac{1}{D\beta}\left(\frac{\partial \tau_y'}{\partial x}-\frac{\partial \tau_x'}{\partial y}\right). \tag{6.92}$$

This is known as *Sverdrup balance*, named after its discoverer, the Norwegian oceanographer Harald Sverdrup. Thus, where the atmospheric surface winds are cyclonic, the steady response of the ocean is poleward flow, and where they are anticyclonic, the flow is equatorward. Applying this to Figure 6.12b, we have water diverging away from the equator at the location of the warm sea surface temperature anomaly (black contours in Figure 6.12a), implying equatorial upwelling, which would damp down the anomaly. These physics are a key part of the "Recharge Oscillator" theory of ENSO, formulated by Wyrtki (1975) and Wyrtki (1985) and modified by Jin (1997).

Another body of theory, developed by Suarez and Schopf (1988) and Battisti and Hirst (1989), postulates that the development of the eastern Pacific warm anomaly during El Niño excites a westward-propagating oceanic Rossby wave that partially reflects off the western boundary, returning eastward as a Kelvin wave that lifts the thermocline in the eastern Pacific, reversing

the warm anomaly. This is known as the “delayed oscillator model” of ENSO. A variant on this idea, also involving partial reflection of eastward-propagating Kelvin waves off the eastern boundary as westward propagating Rossby waves, was proposed by Picaut et al. (1997).

The mechanisms described above are by no means mutually exclusive, and the physics behind them are contained in reduced ENSO models, such as the model developed by Cane and Zebiak (1985), which has proven modestly successful in forecasting El Niño events (Cane et al., 1986). It would probably be premature to claim that we have a reasonably complete understanding of ENSO physics at the time of this writing, and further progress is likely to depend on better understanding of tropical atmospheric physics and dynamics, ocean dynamics, and air-sea coupling.

References

Battisti, D. S., and A. C. Hirst, 1989: Interannual variability in a tropical atmosphere–ocean model: Influence of the basic state, ocean geometry and nonlinearity. *Journal of Atmospheric Sciences*, **46,** 1687-1712, doi:10.1175/1520-0469(1989)046<1687:Iviata>2.0.Co;2.

Bjerknes, J., 1969: Atmospheric teleconnections from the equatorial pacific. *Mon. Wea. Rev.*, **97,** 163-172, doi:10.1175/1520-0493(1969)097<0163:Atftep>2.3.Co;2.

Cane, M. A., and S. E. Zebiak, 1985: A theory for El Niño and the Southern Oscillation. *Science*, **228,** 1085-1087, doi:10.1126/science.228.4703.1085.

Cane, M. A., S. E. Zebiak, and S. C. Dolan, 1986: Experimental forecasts of El Niño. *Nature*, **321,** 827-832, doi:10.1038/321827a0.

Federov, A. V., and J. N. Brown, 2009: Equatorial waves. *Encyclopedia of ocean sciences*, J. Steele, Ed., Academic, San Diego 3679=3695 pp.

Gill, A. E., 1980: Some simple solutions for heat-induced tropical circulation. *Quart. J. Roy. Meteor. Soc.*, **106,** 447-462, doi:https://doi.org/10.1002/qj.49710644905.

Jin, F.-F., 1997: An equatorial ocean recharge paradigm for ENSO. Part I: Conceptual model. *J. Atmos. Sci.*, **54,** 811-829, doi:10.1175/1520-0469(1997)054<0811:Aeorpf>2.0.Co;2.

Matsuno, T., 1966: Quasi-geostrophic motions in the equatorial area. *J. Meteor. Soc. Japan*, **44,** 25-42.

Picaut, J., F. Masia, and Y. du Penhoat, 1997: An advective-reflective conceptual model for the oscillatory nature of the ENSO. *Science*, **277,** 663-666, doi:10.1126/science.277.5326.663.

Suarez, M. J., and P. S. Schopf, 1988: A delayed action oscillator for ENSO. *Journal of Atmospheric Sciences*, **45,** 3283-3287, doi:10.1175/1520-0469(1988)045<3283:Adaofe>2.0.Co;2.

Takahashi, K., A. Montecinos, K. Goubanova, and B. Dewitte, 2011: ENSO regimes: Reinterpreting the canonical and modoki El Niño. *Geophys. Res. Lett.*, **38**, doi:https://doi.org/10.1029/2011GL047364.

Thomson, W., 1880: On gravitational oscillations of rotating water. *Proceedings of the Royal Society of Edinburgh*, **10,** 92-100, doi:10.1017/S0370164600043467.

Wang, C., C. Deser, J.-Y. Yu, P. DiNezio, and A. Clement, 2017: El Niño and Southern Oscillation (ENSO): A review. *Coral reefs of the eastern tropical Pacific: Persistence and loss in a dynamic environment*, P. W. Glynn, D. P. Manzello, and I. C. Enochs, Eds., Springer Netherlands, Dordrecht 85-106 pp.

Webster, P. J., 2020: *Dynamics of the tropical atmosphere and oceans.* John Wiley and Sons, Oxford, U.K., 501 pp.

Wyrtki, K., 1975: El Niño—the dynamic response of the equatorial Pacific oceanto atmospheric forcing. *J. Phys. Ocean.*, **5,** 572-584, doi:10.1175/1520-0485(1975)005<0572:Entdro>2.0.Co;2.

——, 1985: Water displacements in the Pacific and the genesis of El Nino cycles. *J. Geophys. Res. Oceans*, **90,** 7129-7132, doi:https://doi.org/10.1029/JC090iC04p07129.

Yanai, M., and T. Maruyama, 1966: A stratosphere wave propagating over the equatorial Pacific ocean. *J. Meteor. Soc. Jap.*, **44,** 291-294.